Molecular Modeling of Crystalline Alkylthiophene Oligomers and Polymers

ARTICLE *in* THE JOURNAL OF PHYSICAL CHEMISTRY B · FEBRUARY 2010

Impact Factor: 3.3 · DOI: 10.1021/jp9106124 · Source: PubMed

5 AUTHORS, INCLUDING:

Margherita Moreno
ENEA
18 PUBLICATIONS **414** CITATIONS
SEE PROFILE

Guido Raos
Politecnico di Milano
92 PUBLICATIONS **1,756** CITATIONS
SEE PROFILE

Stefano Valdo Meille
Politecnico di Milano
192 PUBLICATIONS **4,053** CITATIONS
SEE PROFILE

Riccardo Po
Research Center for Renewable Energies & …
113 PUBLICATIONS **1,653** CITATIONS
SEE PROFILE

Molecular Modeling of Crystalline Alkylthiophene Oligomers and Polymers

Margherita Moreno,[†] Mosè Casalegno,[†] Guido Raos,*[,†] Stefano V. Meille,[†] and Riccardo Po[‡]

Dipartimento di Chimica, Materiali e Ingegneria Chimica "G. Natta", Politecnico di Milano, Via L. Mancinelli 7, 20131 Milano, Italy, and Research Center for Non-Conventional Energies, Istituto Donegani, ENI S.p.A, Via Fauser 4, 28100 Novara, Italy

Received: November 6, 2009; Revised Manuscript Received: December 17, 2009

We present the results of a thorough molecular modeling study of several alkylthiophene-based oligomers and polymers. In particular, we consider two polymers whose limit-ordered crystal structures have been recently reported by our group, on the basis of powder X-ray data analysis: poly(3-(*S*)-2-methylbutylthiophene) (P3MBT) and form I′ of poly(3-butylthiophene) (P3BT). We first describe the development of a series general purpose force fields for the simulation of these and related systems. The force fields incorporate the results of ab initio calculations of the bond torsion energies of selected oligomers and differ in the set of atomic charges used to represent the electrostatic interactions. We then present the results of an extensive validation of these force fields, by means of molecular mechanics (MM) energy minimizations and molecular dynamics (MD) simulations of the crystal structures of these oligomers and polymers. While our "best" force field does not outperform the others on each of the investigated systems, it provides a balanced description of their overall structure and energetics. Finally, our MM minimizations and MD simulations confirm that the reported crystal structures of P3MBT and P3BT are stable and correspond to well-defined energetic minima. The room-temperature MD simulations reveal a certain degree of side-chain disorder, even in our virtually defect-free polymer crystal models.

1. Introduction

Poly(3-alkylthiophenes) (P3AT) and thiophene-based oligomers represent an important class of organic semiconducting materials.[1–7] Because of their attractive combination of high charge mobility, luminescence, environmental stability, and processability in common organic solvents, they are being widely employed in a number of devices such as thin film transistors,[8] light-emitting diodes,[9] chemical or biological sensors,[10] and photovoltaic cells.[11] The performance of these devices is known to be affected by several structural and morphological parameters, such as the degree of crystallinity, the average size and orientation of the crystallites with respect to the supporting material, and the formation of specific polymorphs. In turn, these depend on the structure of the monomer units, the regioregularity and molecular weight distribution of the polymer, the deposition method (usually casting or spin coating), and postdeposition treatments such as thermal or solvent annealing. In many instances, there is at least a qualitative understanding of these factors. For example, the identification of regioregular poly(3-hexylthiophene) (P3HT) as the "material of choice" for many applications is the result of a compromise between processability (which increases with the length of the alkyl side chains) and the efficiency of change transport (which presumably decreases with it, other things being equal). However, most researchers would agree that real quantitative understanding is still lacking. This is of course crucial, if we eventually want to approach the goal of designing devices based on these materials, starting from the molecular level. Until the development of such quantitative design principles, it is unlikely that the potential of organic semiconducting materials will be fully exploited.

The advantage of having a detailed model of the solid-state organization of P3AT's is almost self-evident, for example to those interested in elucidating the driving forces which guide their crystallization, self-assembly, and interaction with substrates,[4,5,8,11] or in modeling their excitation and charge transport processes at the quantum mechanical level.[12,13] Until recently, such information has been hard to come by. As a result of the poor quality of the available X-ray diffraction data, which is related to the relatively high disorder and low propensity to crystallization of these polymers (even when they are highly regioregular), the solid-state organization of P3AT's has generally been described by semiquantitative models.[14] At this level, their crystal structures can be simply described in terms of π-stacked layers of parallel chains, which are then placed on top of each other, at a distance that depends on the length of their side chains and the type of polymorph. The latter have been broadly classified in two classes, termed type-I and type-II, depending on the position of the X-ray peaks corresponding to intralayer and interlayer diffraction. The work of Arosio et al.[15] on poly(3-*S*-methylbutylthiophene) (P3MBT) contains the first well-defined structural model for a (semi)crystalline P3AT, with a full specification of the unit cell, space group, and fractional coordinates of all the heavy atoms. This work was based on the construction of acceptable starting models on the basis of packing and symmetry arguments, and their refinement by Rietveld analysis[16] of the powder X-ray diffraction profiles. In this particular case, the preliminary analysis of the viable models was simplified by the presence of the chiral side chains, which automatically ruled out all the space groups with symmetry planes or inversion centers. Things become more complicated when these symmetry elements are admissible, as in the case of the P3AT's with linear side chains. Thus,

* Corresponding author. E-mail: guido.raos@polimi.it. Phone: +39-02-2399-3051. Fax: +39-02-2399-3080.
[†] Politecnico di Milano.
[‡] Istituto Donegani.

10.1021/jp9106124
Published on Web 01/08/2010

subsequent work by our group on poly(3-butylthiophene) (P3BT)[17] used the same tools with an additional support by molecular modeling. In particular, we performed energy minimization on different candidate structures. Eventually, we succeeded in identifying a well-defined "limit-ordered model"[18] for the so-called form I′ of this polymer. Its is noteworthy that both P3MBT and form I′ of P3BT are characterized by similar unit cells and chain packing modes, according to the orthorhombic $C222_1$ space group.

The present article extends our previous work on these systems[15,17] by providing a more in-depth analysis by molecular modeling methods.[19–22] To be successful, any application of the molecular mechanics (MM) and classical molecular dynamics (MD) methods requires a careful parametrization of the intramolecular degrees of freedom and of nonbonded interactions.[23] Thus, we start by describing a general purpose force field (FF) for the simulation of thiophene-based polymers and oligomers. In fact, we have developed and tested several related force fields: the reasons for this will be discussed here in some detail.

A number of FF's for thiophene-based materials have been described and used by us[24,25] as well as others:[26–30] see ref 26b for a review of recent simulation work. Applications include the structure and energetics of crystal surfaces and adsorbed monolayers,[25,26a] the self-assembly of hybrid thiophene−peptide copolymers ("molecular chimeras"),[26b] and the elucidation of the electronic states in neutral or charged polythiophenes[27,28] (in these last cases, snapshots extracted from MD simulations were used as an input for subsequent quantum mechanical calculations). Some authors have attempted the simulation of the amorphous polymers.[28,29] Here, instead, we concentrate on the description of well-defined polymer and oligomer crystal structures. In our experience, the reproduction of these crystal structures represents a rather severe test of the quality of a FF.

The present FF differs from our previous one[24] both in several specific details and in its general philosophy. In particular, in our previous attempt we developed a whole set of dedicated FF's, one for each of the oligomers that was investigated. Thus, we did not worry much about the transferability from molecule to molecule of parameters such as the atomic charges. Here, instead, we have sought to develop a "plug and play" FF, which could be used without further adjustments on any possible combination of thiophene backbones and alkyl side chains.

In the following section we present the FF parameter sets. In section 3 we test them, by comparing the results of MM minimization of the crystal structures of several thiophene-based oligomers and the P3BT and P3MBT polymers. In section 4 we illustrate their suitability also for MD simulations, considering as an example these two polymers and two oligomer crystal structures. Conclusions follow.

2. Force Field Parametrization

2.1. Generalities. A FF represents the potential energy of a molecular system by a simple functional form, depending through several empirical parameters on the coordinates of its nuclei.[20,21,31] In this work, we have adopted the following standard expression, borrowed from OPLS-AA[32] and other "class 1" force fields such as CHARMM[33] and AMBER:[34]

$$V_{FF}(\mathbf{r}_1, \mathbf{r}_2, ..., \mathbf{r}_N) = \sum_{\text{bonds}} \frac{1}{2}K_b(b - b_0)^2 + \sum_{\text{angles}} \frac{1}{2}K_\theta(\theta - \theta_0)^2 + \sum_{\substack{\text{improper}\\ \text{dihedrals}}} \frac{1}{2}K_\xi(\xi - \xi_0)^2 + \sum_{\text{dihedrals}} \frac{1}{2}K_\varphi[1 + \cos(n\varphi - \delta_n)] + \sum_{i<j} \left\{4\varepsilon_{ij}\left[\left(\frac{\sigma_{ij}}{r_{ij}}\right)^{12} - \left(\frac{\sigma_{ij}}{r_{ij}}\right)^{6}\right] + \frac{q_i q_j}{\kappa r_{ij}}\right\} \quad (1)$$

During the development of the FF, our decisions were guided by a few general principles. First of all, we wanted to ensure compatibility and transferability of parameters among related oligo- and polythiophenes. Second, a full reparametrization was beyond the purpose of our study and would have required a large number of compounds and benchmark data (either from experiment or ab initio calculations). Thus, whenever possible, we adopted the conservative strategy of borrowing important parameters from the OPLS-AA force field.[32] For the same reasons, we decided from the outset to retain as much as possible the original OPLS-AA parametrization for the alkyl side chains.

The first two terms in eq 1 are straightforward. They represent the energies associated with bond stretching and angle bending, in the harmonic approximation. The equilibrium values of the bond lengths and bond angles (b_0 and θ_0, respectively) can be easily obtained from the available crystal structures or from ab initio calculations on a few thiophene oligomers (see below). The associated force constant can in principle be derived from the vibrational spectra, either experimental (IR and Raman) or calculated ab initio. However, any serious attempt to reproduce these vibrational spectra would require additional potential energy contributions, such as the anharmonic and bend−stretch cross terms included by "class 2" FF's such as Allinger's MM3.[35] In addition, in the specific case of polyconjugated systems such as those considered here, some of these force constants would be quite sensitive to the overall chain length, as a consequence of the delocalization of its π electrons.[36] Since we are interested in modeling the conformation and packing of the chains and these features are expected to be relatively insensitive to short-time vibrational effects, we have bypassed altogether this problem by borrowing standard values of these force constants from OPLS-AA (whose authors, in turn, borrowed them from AMBER). In the MD simulations, we actually kept the C−H bond distances fixed at their equilibrium values, since eliminating their fast vibrations allows the use of longer time steps in the integration of the equations of motion.

The third term in the FF expression contains the improper dihedrals, whose main purpose is simply to ensure that sp^2 carbons remain planar. Also in this case we have borrowed standard parameter values from OPLS-AA. The last terms in eq 1 represent the torsion energies and the nonbonded interactions, respectively. These are extremely important, given our objective of modeling the crystal structures and phase behavior of P3AT's. Therefore, the remaining part of this section is entirely devoted to the discussion of its parametrization and testing.

Before we go on with the discussion of the molecular mechanics parameters, it is important to establish a clear distinction between *atom classes* and *atom types*. There may be several atom types associated with a certain atom class. The atom class determines the bonded parameters and the dispersion-repulsion part of the nonbonded interactions, whereas the atom type determines the electrostatic part of the nonbonded interactions (atomic charges).

All MM and MD simulations were conducted with the TINKER 4.2 molecular modeling program.[37] A TINKER-style

TABLE 1: Diagonal (Same Atom) LJ Parameters for Our Force Fields[a]

atom class code	description	ε_{ii} (kcal mol^{-1})	σ_{ii} (Å)
ST	thiophene sulfur	0.250	3.55
CSA	thiophene α carbon	0.070	3.55
CSB	thiophene β carbon	0.070	3.55
CSR	aliphatic carbon bonded to thiophene	0.066	3.50
CT	generic aliphatic carbon	0.066	3.50
HCS	hydrogen bonded to thiophene	0.030	2.42
HC	generic aliphatic hydrogen	0.030	2.50

[a] Atom names correspond to those depicted in Figure 1.

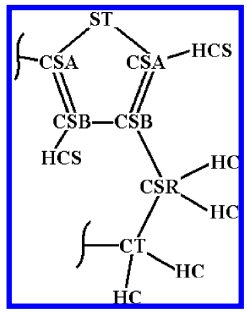

Figure 1. Structure and atom class definitions for a generic alkylthiophene fragment.

file with a complete parameter set is provided in the Supporting Information. All ab initio calculations were carried out with the GAMESS-US program.[38]

2.2. Repulsion−Dispersion Interactions. According to eq 1, the pairwise short-range repulsion and the dispersion interactions are described by the Lennard-Jones (LJ) functional form. All the LJ parameters were taken from related atom classes within OPLS-AA. For the reader's convenience, the diagonal terms σ_{ii} and ε_{ii} have been collected in Table 1, while the atom class definitions are illustrated in Figure 1. For consistency, we have also adopted OPLS-AA's combination rules for the LJ parameters, whereby $\varepsilon_{ij} = (\varepsilon_{ii}\varepsilon_{jj})^{1/2}$ and $\sigma_{ij} = (\sigma_{ii}\sigma_{jj})^{1/2}$. Note, however, that there is no rigorous theoretical justification for these mixing rules,[23] and their adoption has sometimes negative consequences. In our own work, for example, we have encountered one particular situation in which they lead to an incorrect prediction for the sign of the excess volume of mixing of two liquids (water and the room-temperature ionic liquid [Bmim][BF_4]).[39] These nonbonded interactions act between sites in different molecules but also between sites belonging to the same molecule, separated by three or more bonds. For atom pairs separated by exactly three bonds (1−4 interactions), following again OPLS-AA, a factor of 0.5 is used to rescale both the LJ and Coulomb interactions.

In a previous study,[24] we relied on the MM3 parametrization[35] to represent the dispersion−repulsion interactions. MM3 uses a Buckingham-type (exp-6) potential to represent them, which is in principle more accurate than the LJ form. However, the parameters entering them are not as thoroughly tested as those of OPLS-AA. Therefore, in that case we found that some parameter changes were necessary, and even so we could not reproduce both the crystal structures and the heats of sublimations of the oligomers in a fully satisfactory way. Here instead, following our subsequent experience with α-quaterthiophene (T4),[25d] we will show that the LJ parameters from OPLS-AA provide good agreement with the available experimental data, without any further adjustments.

2.3. Electrostatic Interactions. Although weak compared to more polar organic compounds (alcohols, carboxylic acids, etc.), electrostatic interactions play an important role in determining the crystalline organization of π-conjugated systems. The characteristic herringbone arrangement adopted by many aromatic compounds in the solid state depends on their quadrupolar charge distribution, which to a first approximation can be described in terms of positively charged hydrogens and negatively charged carbons (the latter represent the electron-rich π-conjugated system). In addition, unlike benzene, thiophene has of course a nonzero dipole moment (0.55 D[40]). The importance of these electrostatic interactions has been confirmed also by accurate quantum chemical calculations on the thiophene van der Waals dimer, in the gas phase.[41]

Some time ago,[24] we investigated different models for the electrostatic interactions in crystalline oligothiophenes. We tested the performance of point-change models against a more sophisticated description based on a distributed multipole analysis (DMA).[23] Here, instead, we have directly taken the point-change model represented by the Coulomb term in eq 1 as our starting point.

We investigated several distinct sets of point charges. Here we shall describe only a few models. The first one will be denoted by FF1 and was built directly on the OPLS-AA parametrization for related compounds. In saturated hydrocarbons, this FF places a charge of +0.060 (in units of elementary charges e) on each hydrogen bonded to an sp^3 carbon. To keep each group electrically neutral, each carbon atom acquires a charge of $-0.060n_H$, where n_H is the number of hydrogens directly bonded to it (3, 2, and 1 for methyl, methylene, and methine, respectively). These charges were adopted without modification for the alkyl chains attached to the thiophene backbones. Conversely, in unsaturated hydrocarbons (either alkene or aromatic), a hydrogen bonded to an sp^2 carbon has a charge of +0.115, and correspondingly the carbon acquires a charge of $-0.115n_H$. To extend this simple parametrization to thiophene-based molecules, we adopted the charge scheme illustrated in Figure 2. As can be seen, we assigned the standard charges to the four hydrogens and to the two β carbons of thiophene. We then placed a charge δ on the S atom, and a charge $-0.115 - \delta/2$ on each of the two α carbons to preserve overall electroneutrality. The value of $\delta = +0.018$ was chosen to reproduce the experimental gas-phase dipole moment of thiophene, at its equilibrium geometry.

A positive charge on thiophene's sulfur might seem surprising at first, but in fact the electronegativity of S is slightly lower than that of C on the Pauling scale. This is confirmed also by the point charges of an isolated thiophene molecule, obtained by fitting[42] the molecular electrostatic potential (ESP) calculated from the B3LYP/6-311G** charge distribution.[22] In fact, we see that the ab initio calculation place an even more positive charge on the sulfur. More generally, the ab initio calculations lead to a higher degree of charge separation (somewhat more positive hydrogens and more negative carbons, on average), but in spite of these differences this model also produces quite reasonable values for the molecular dipole moment (0.475 D

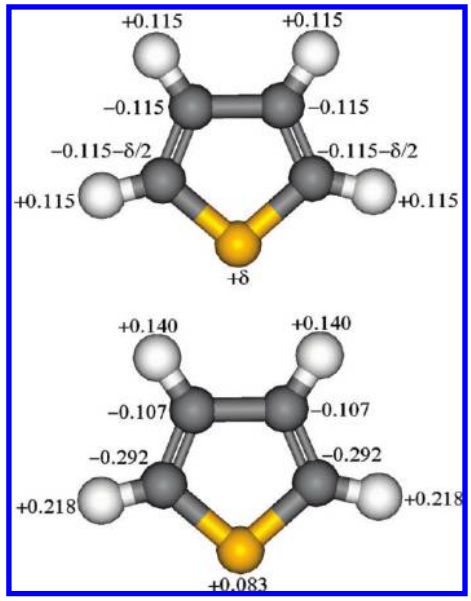

Figure 2. Charge schemes for the thiophene molecule. Top: simple OPLS-AA-style charge assignment, where $\delta = +0.018$ (see text). Bottom: atomic charges derived from a fit of the ab initio molecular electrostatic potential (B3LYP/6-311G**).

for the dipole moment calculated from the full electron density, 0.502 D for the dipole moment calculated from the ESP point charges).

The greatest strength of the FF1 charge model is its simplicity and transferability. The atomic charges on any oligo- or poly(alkylthiophene) can be assigned in a straightforward way from these values, assuming their transferability and remembering that, whenever a hydrogen atom of thiophene is removed and replaced by a carbon (belonging to another thiophene ring or to a pendant alkyl chain), its charge must be summed back onto its original carbon to preserve local electroneutrality.

A second set of atomic point charges was derived by a fit of the molecular electrostatic potential,[42a] calculated ab initio at the B3LYP/6-311G** level.[22] The resulting "potential-derived charges" (PDC) are very close to those from the popular CHELPG method,[42b] which is indeed very similar to it. The associated force field will be denoted by FF2. In addition to the thiophene molecule, four oligomers were chosen for these calculations and they are shown in Figure 3. They represent the main situations which can be encountered for alkyl-substituted oligomers and polymers. For thiophenes located at the chain terminals, we have (i) no alkyls, (ii) one alkyl in α position, and (iii) one alkyl in β position. For thiophenes in the interior of a chain, we have (iv) no alkyls, (v) one alkyl in β position, and (vi) two alkyls in β position. Clearly, case (v) is the only important one for the description of P3AT's of high molecular weight, where chain-end effects are negligible. The other cases, in particular (i)−(iii), are relevant for the oligomers.

The atomic charges produced by the PDC algorithm were slightly adjusted to ensure their transferability. First, we kept the number of atom types to a reasonably low number by averaging the charges of "similar" atoms. Second, we imposed that the charges of the atoms belonging to a thiophene monomer unit (including any pendant side chain) must always add up to zero. In this way, it is possible to form a polymer or an oligomer by concatenating any of these units in any order, without having to readjust the charges to ensure overall neutrality of the molecules. Third, we kept the standard OPLS-AA charges for the alkyl carbons and hydrogens, with the exception of the carbon atoms directly bonded to the thiophene rings (CSR class) which were allowed to take different values, to allow for the possibility of some charge transfer between the alkyl chains and the conjugated backbone. The results of this process are collected in Table 2.

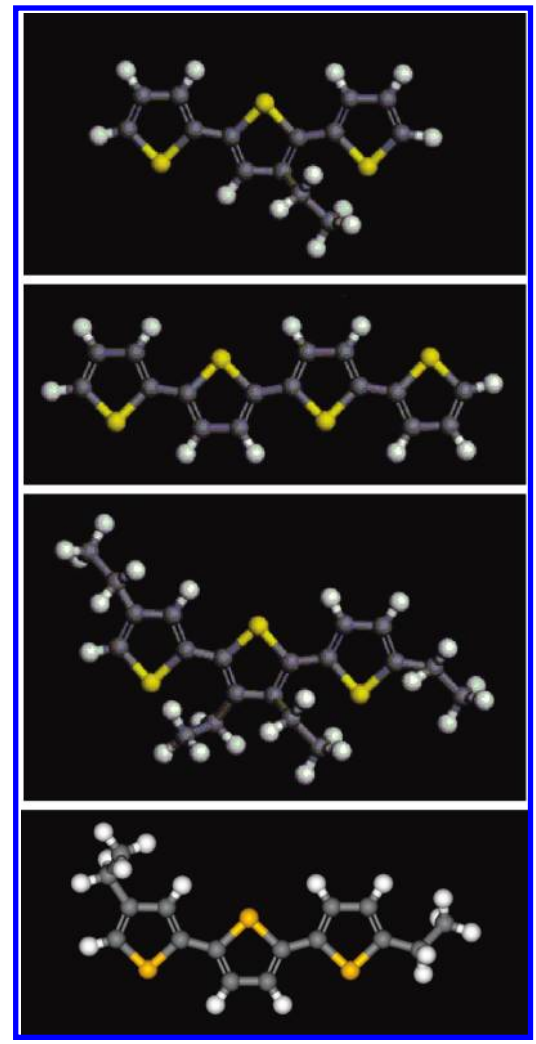

Figure 3. Thiophene oligomers chosen for the calculation of the atomic point charges by fitting of the ab initio molecular electrostatic potential.

Comparing the atomic charges for FF1 and FF2, we see that the latter have a certain variability to account for different local environments. In particular, within FF2 the thiophene rings acquire a small negative charge in alkylthiophenes, which is compensated by a small positive charge on the CH_2 group directly bonded to it. This effect can be ascribed to "hyperconjugation" (a well-known effect in organic chemistry) or to the higher electronegativity of $C(sp^2)$ compared to $C(sp^3)$. Within our charge scheme, this extra negative charge is assigned mainly the S atom, which thus switches from being slightly positive in isolated thiophene to slightly negative in poly(3-alkylthiophenes).

The last column in Table 3 contains a third set of atomic charges, which were used to define force field FF3. These atomic charges are simply the arithmetic averages of the atomic charges defined within FF1 and FF2. This somewhat unconventional choice was taken as a pragmatic solution to the observation (see below) that FF1 and FF2 seem to slightly underestimate and overestimate the intermolecular interactions, respectively.

In all our simulations, we neglected both LJ and electrostatic nonbonded interactions beyond a cutoff distance of 12 Å, using

TABLE 2: Atomic Point Charges for Force Fields FF1, FF2, and FF3, for Each Atom Type (See Table 1 for the Atom Classes)

atom class	atom type description	FF1	FF2	FF3
ST	S, inner thiophene, no alkyls	+0.0180	+0.0000	+0.0090
	S, inner thiophene, one alkyl in β	+0.0180	−0.1200	−0.0510
	S, terminal thiophene, no alkyls	+0.0180	+0.0600	+0.0390
	S, terminal thiophene, one alkyl in β	+0.0180	−0.0300	−0.0060
	S, terminal thiophene, one alkyl in α	+0.0180	−0.1600	−0.0710
CSA	C_α of thiophene, bonded to thiophene	−0.0090	0.0000	−0.0045
	C_α of thiophene, bonded to hydrogen	−0.1240	−0.2400	−0.1820
	C_α of thiophene, bonded to alkyl	−0.0090	+0.0400	+0.0155
CSB	C_β of inner thiophene, bonded to hydrogen	−0.1150	−0.1800	−0.1475
	C_β of inner thiophene, bonded to alkyl	0.0000	−0.0300	−0.0150
	C_β of terminal thiophene, bonded to hydrogen	−0.1150	−0.1800	−0.1475
	C_β of terminal thiophene, bonded to alkyl	0.0000	−0.0300	−0.0150
CSR	R*C*H$_2$C$_\beta$ of inner thiophene	−0.1200	+0.0300	−0.0450
	R*C*H$_2$C$_\beta$ of terminal thiophene	−0.1200	0.0000	−0.0600
	R*C*H$_2$C$_\alpha$ of terminal thiophene	−0.1200	0.0000	−0.0600
CT	alkyl R*C*H$_3$	−0.1800	−0.1800	−0.1800
	alkyl R$_2$*C*H$_2$	−0.1200	−0.1200	−0.1200
	alkyl R$_3$*C*H	−0.0600	−0.0600	−0.0600
HC	alkyl hydrogen	+0.0600	+0.0600	+0.0600
HCS	thiophene hydrogen	+0.1150	+0.1800	+0.1475

TABLE 3: Summary of the Minimization Results, Providing the Overall *F* Values (See Eq 2) for Each Crystal Structure and Force Field

structure	FF1	FF2	FF3
(**1**) PEWXAQ01	28.7	26.7	26.2
(**2**) PEWXAQ02	180.4	67.4	129.2
(**3**) ZAQZUM	31.1	24.4	26.2
(**4**) ZAQZUM01	191.4	28.2	74.3
(**5**) LIWRAK	94.9	87.0	92.1
(**6**) LIWRAK01	15.7	21.5	17.9
(**7**) FIYVIT	12.6	7.0	9.5
(**8**) XASBOJ	81.9	12.8	38.2
(**9**) LIMGUJ	208.6	163.7	182.6
(**10**) P3BT	28.4	25.9	22.1
(**11**) P3MBT	47.5	106.1	57.5

a suitable truncation scheme to ensure smoothness of the potential energy function. In our experience Ewald-type summation schemes, which compute exactly all long-range Coulomb interactions in systems with periodic boundary conditions, are unnecessary in these systems with relatively small atomic charges.

2.4. Torsion Energies. The final missing part in the FF definition is represented by the bond torsion energies. Since intramolecular 1−4 interactions contribute significantly to the overall torsion energy about a specific bond, the parameters entering the "intrinsic" torsion energy (represented by the Fourier terms within eq 1) must be determined after choosing the LJ and electrostatic parameters. In particular, being associated with different sets of point charges, each FF must have *different intrinsic* torsion parameters, in order to reproduce the *same overall* torsion energy.

Consistent with our strategy of relying as much as possible on OPLS-AA, the torsion parameters for the intraring bonds (essentially required to keep the thiophenes planar) and the "outer" bonds of the alkyl side chains (*−CT−CT−* and *−CSR−CT−*) were directly taken from this force field. Instead, the torsion energies about the inter-ring bond (defined by the ST−CSA−CSA−ST dihedral angle) and about the bonds connecting the alkyls to the thiophene moieties (CT−CSR−CSB−CSA for alkyls in β position, CT−CSR−CSA−CSB for alkyls in α position) were reparametrized in each case in order to reproduce the ab initio energies. Systematic ab initio investigations of the bithiophene torsion potential were carried out in a previous work,[43] where it was concluded that the B3LYP hybrid density functional complemented with a 6-311G** basis set is a good compromise between computational cost and accuracy of the results.

In Figure 4 we have collected the final potential energy curves (including the intrinsic one for force field FF2) for the following cases:

(a) the central torsion of α-quaterthiophene (keeping the two outer torsions locked in the trans-planar state), which has been used to parametrize the inter-ring torsions in the oligo- and polythiophenes;

(b) the thiophene−alkyl torsion of 2-ethylthiophene, which has been used to parametrize the first terminal-chain torsion in α-substituted oligothiophenes;

(c) the thiophene−alkyl torsion of 3-ethylthiophene, which has been used to parametrize the first side-chain torsion in β-substituted oligo- and polythiophenes.

Very briefly, the steps followed to obtain an intrinsic torsion potential are as follows:

(1) calculate the reference B3LYP/6-311G** data by constrained minimizations of the system's energy, scanning the relevant degree of freedom at evenly spaced points (we used a 30° spacing, from 0° to 180°);

(2) compute the MM energy for the same set of points, after setting to zero all the Fourier coefficients of the relevant intrinsic torsion potential;

(3) obtain the intrinsic torsion potential from the difference of the potential energies calculated in steps (1) and (2), and interpolate it a Fourier series;

(4) insert this intrinsic potential in the MM parameter file, and compute the "full" potential energy curve. If every step has been carried out correctly, this curve should coincide with the ab initio curve calculated in step (1).

Figure 4 illustrates the difference between the full and the intrinsic MM potential energy curves, which as discussed above are due to the contribution of intramolecular nonbonded interactions.

Before leaving this section, let us comment briefly the final torsion energy curves. These functions, which are even and have a period of 360°, are plotted in Figure 4 for torsion angles comprised between 0° and 180°. The torsion energies for the alkyl chains show that these groups tend to stand approximately orthogonal to the thiophene plane. However, in both cases (α-

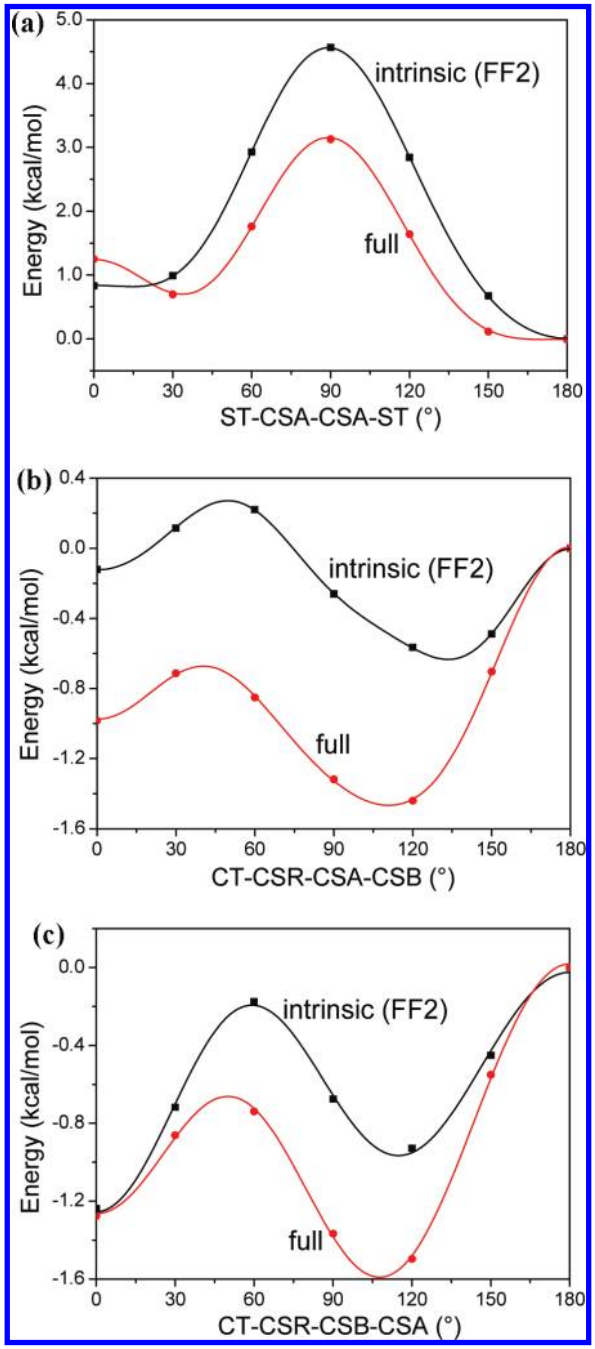

Figure 4. Bond torsion energies. From top to bottom: (a) torsion about a thiophene−thiophene $C_\alpha-C_\alpha$ bond; (b) torsion about a thiophene−alkyl $C_\alpha-C(sp^3)$ bond; (c) torsion about a thiophene−alkyl $C_\beta-C(sp^3)$ bond. The "full" potential energy curves (red) correspond both to the ab initio B3LYP/6-311G** energies and to the final MM energies, after inserting the appropriate "intrinsic" potential (black) within the force field.

and β-substitution) there is a second local minimum at 0° which is fairly close in energy (0.5−0.8 kcal/mol). This minimum corresponds to a planar conformation which, in the solid state, may be actually preferred over the orthogonal one because of molecular packing forces. The curve for the interthiophene torsion shows an absolute minimum corresponding the trans-planar state (ST−CSA−CSA−ST = 180°). The potential energy profile about this minimum is quite flat, which means that this angle may easily distort away from planarity if this is required to optimize other intra- and intermolecular interactions. There is also a second local minimum corresponding to a cis-distorted state at ST−CSA−CSA−ST = 30°. At 90° there is a barrier of 2.5−3.0 kcal/mol separating the trans from the cis minima.

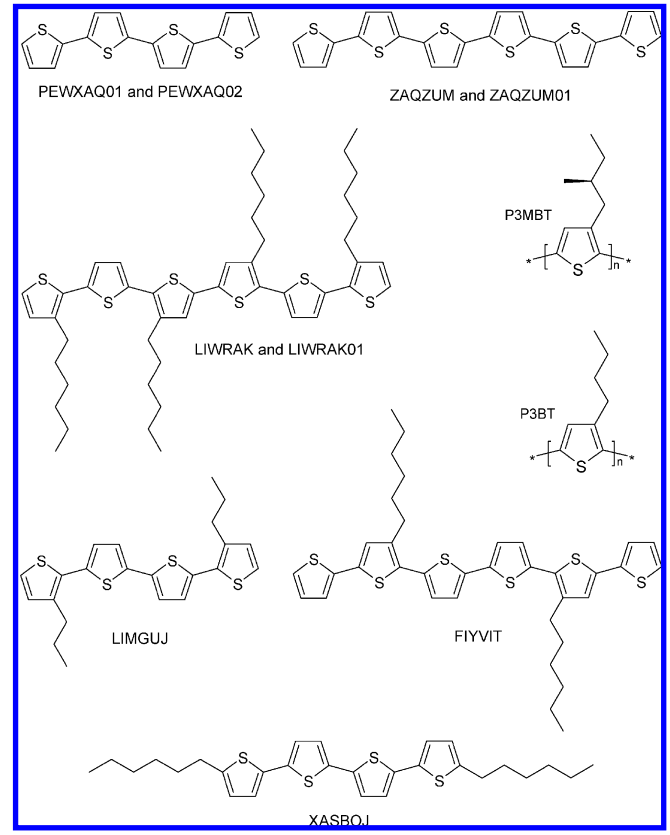

Figure 5. Molecular structures of the thiophene oligomers and polymers.

Note that, in our previous simulation work, we relied on a high-level ab initio potential energy curve for bithiophene (calculated at the MP2/aug-cc-pVTZ level).[43] Compared to the present torsion potential, the previous one had a lower 90° barrier and a slightly higher tendency to distort away from planarity toward a trans-distorted state. This had some unwanted structural consequences, according to a preliminary set of test calculations on oligothiophene crystals (see below). These differences can be justified by the different types of ab initio calculation (MP2 vs B3LYP), but also by the fact that the thiophene tetramer has a more extensive conjugation than the dimer. Indeed, other authors[44] observed a slight but quite systematic trend toward greater coplanarity and a higher torsional barrier at 90°, on going to increasingly longer oligomers. The adoption of a torsion potential calculated on the tetramer appeared to us as a reasonable compromise between the computational requirements and the need of a reasonable (albeit imperfect) description for all alkylthiophene oligomers and polymers.

3. Force Field Validation

To validate our force fields, we applied them to the minimization of the crystal forms of a few representative oligo- and polythiophenes, both with and without pendant alkyl chains (see Figure 5 for the sketches of their chemical structures):

(1) the "low-temperature" form of α-quaterthiophene (code PEWXAQ01[45] on the Cambridge Structural Database[46]);

(2) the "high-temperature" form of α-quaterthiophene (PEWX-AQ02[45] on the CSD);

(3) the "low-temperature" form of α-sexithiophene (ZAQ-ZUM[47] on the CSD);

(4) the "high-temperature" form of α-sexithiophene (ZAQ-ZUM01[48] on the CSD);

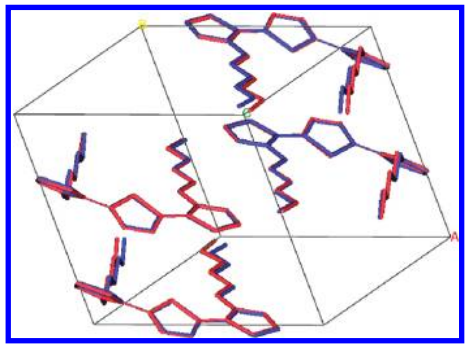

Figure 6. A view of a 2 × 1 × 1 supercell of LIWRAK. The experimental structure is shown in blue, while the calculated structure is shown in red (minimization with fixed lattice parameters, force field FF2). The molecules are divided in two fragments in this view.

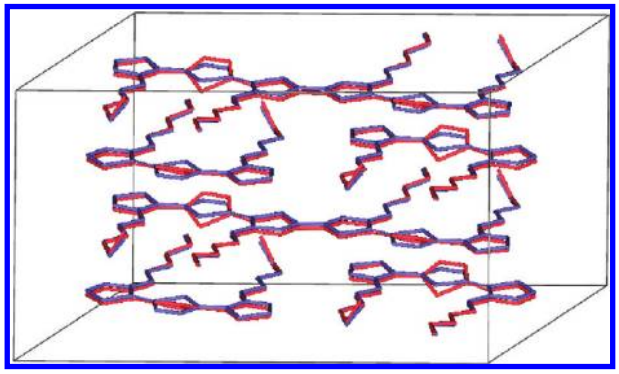

Figure 7. A view of a 1 × 2 × 1 supercell of LIWRAK01. The experimental structure is shown in blue, while the calculated structure is shown in red (minimization with fixed lattice parameters, force field FF2). Some molecules are divided in two fragments in this view.

(5) the "yellow" form of 3,3″,4‴,3⁗,5⁗-tetrahexyl-2,2′:5′,2″:5″,2‴:5‴,2⁗:5⁗,2⁗′:5⁗′,2′′′′′-sexithiophene (LIWRAK[49] on the CSD);

(6) the "red" form of 3,3″,4‴,3⁗,5⁗-tetrahexyl-2,2′:5′,2″:5″,2‴:5‴,2⁗:5⁗,2⁗′:5⁗′,2′′′′′-sexithiophene (LIWRAK01[50] on the CSD);

(7) 4′,3⁗-di-*n*-hexyl-2,2′:5′,2″:5″,2‴:5‴,2⁗:5⁗,2⁗′:5⁗′,2′′′′′-sexithiophene (FIYVIT[51] on the CSD);

(8) α,ω-dihexyl-all-antiquaterthiophene (XASBOJ[52] on the CSD);

(9) 3,3‴-dipropyl-2,2′:5′,2″:5″,2‴-quaterthiophene (LIMGUJ[53] on the CSD);

(10) the I′ form of regioregular poly(3-butylthiophene) (P3BT[17]);

(11) regioregular poly(3-*S*-methylbutylthiophene) (P3MBT[15]).

Figures 6−9 provide a view of crystal structures **5**, **6**, **10**, and **11**, while the Supporting Information contains all of them. These pictures are meant to give a qualitative idea of the structural motifs encountered in these systems and of overall the quality of the final results.

Depending on the crystal structure under investigation, TINKER's algorithms sometimes (but not always) require all lattice lengths to be greater than 11.0 Å in order to calculate properly all the bonded and nonbonded interactions (this is twice the default value of the POLYMER-CUTOFF parameter within TINKER). In these cases, we simply constructed a small supercell compatible with this constraint by replicating the original unit cell. In all cases (unit cell or supercell calculations), the crystal symmetry specified by the space group is exploited in the initial setup of the calculations, but it is not enforced during the energy minimizations. Nonetheless, we never observed a change in crystal symmetry.

Two successive energy minimizations were performed on each structure. First of all, we performed an "atoms-only" (ao) optimization of the atomic coordinates, keeping the lattice parameters at their experimental values. To this purpose, we employed the NEWTON program of TINKER. The results of this first optimization step have been summarized by the Δ_{rms}(ao) parameter, which is the root-mean-square displacements of the atoms (excluding hydrogens) from their original experimental positions. Starting from this optimized structure, a second "full cell" (fc) minimization was carried out with TINKER's XTALMIN program, which alternates cycles of optimization over the atomic coordinates with optimization over the lattice parameters. The results of both minimizations (Δ_{rms} from ao and final lattice parameters from fc) have been collected in the Supporting Information (Tables S1−S11). Finally, Table 3 contains an overall figure of merit which summarizes the quality of the two calculations:

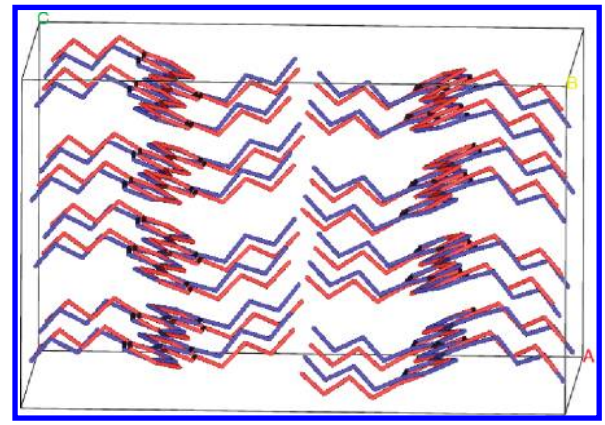

Figure 8. A view of 2 × 2 × 1 supercell of P3BT. The experimental structure is shown in blue, while the calculated structure is shown in red (minimization with fixed lattice parameters, force field FF2).

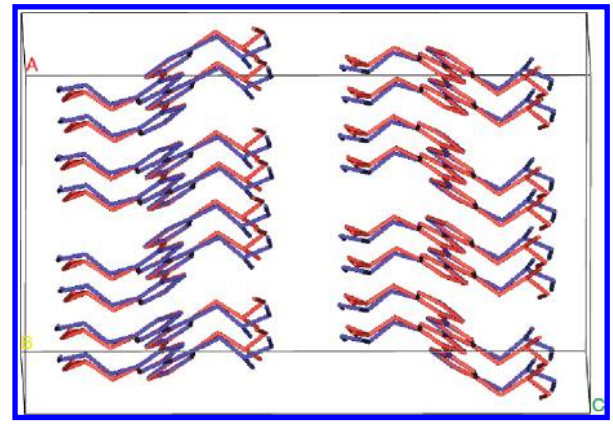

Figure 9. A view of 2 × 2 × 1 supercell of P3MBT. The experimental structure is shown in blue, while the calculated structure is shown in red (minimization with fixed lattice parameters, force field FF2).

$$F = \left[\frac{\Delta_{RMS}(ao)}{d_0}\right]^2 + \sum_{p=1}^{6}\left[100 \times \frac{l_p(fc) - l_p(0)}{l_p(0)}\right]^2 \quad (2)$$

In the second term on the right-hand side, l_p(fc) represents an optimized lattice parameter, while $l_p(0)$ is its experimental value. In the first term, d_0 is a reference displacement which normalizes Δ_{rms}(ao) and converts it into a pure number. The choice of d_0 determines the relative weight of the atomic displacements and of the lattice parameters in the final figure of merit. Here we took $d_0 = 0.1$ Å, to make these contributions roughly comparable on average.

TABLE 4: Comparison of the Experimental and Calculated Heats of Sublimation (in kcal/mol) of α-Quaterthiophene (T4) and α-Sexithiophene (T6), from the Atoms-Only and Full Cell Minimizations of the "Low Temperature" Forms with Both Force Fields

	expt	FF1 (ao)	FF1 (fc)	FF2 (ao)	FF2 (fc)	FF3 (ao)	FF3 (fc)
T4	33.3 ± 1.5	34.7	35.2	38.1	38.8	36.3	36.8
T6	50.0 ± 1.0	51.6	52.0	56.5	57.1	53.9	54.5

We will first discuss the oligomers (structures **1**−**9**) and then move on to consider the two polymers (structures **10** and **11**). According to our results, FF2 is clearly superior to FF1 *as far as the oligomers are concerned*. Force field FF3 systematically produces results which interpolate between those by FF1 and FF2. This is of course expected, given its original definition as the "average" of those force fields. Only in one case (LIWRAK01), the *F* value of FF1 is slightly lower (i.e., better) than that of FF2. FF2 appear to perform equally well on all crystal structures, while FF1 has a more uneven and somewhat unpredictable behavior. FF1 underperforms especially in the prediction of the unit cell parameters (fc minimizations), while it is fairly accurate in the minimizations with fixed lattice parameters. The Δ_{rms}(ao) values obtained from the FF2 minimizations are always lower than 0.24 Å, with the sole exception of the structure LIMGUJ where we obtain Δ_{rms}(ao) = 0.43 Å. Note, however, that this structure was not fully refined by the group which reported it, and indeed the experimental structure contains an unrealistic C−C bond length of 0.915 Å in one of the side chains. Therefore, in this case the disagreement of the FF2 predictions with the experimental data may be attributed to a significant extent to the latter. Visual inspection of the structures demonstrates that this force field reproduces fairly well the conformation of both the conjugated main chains and of the alkyl side chains (see Figures 6 and 7, for example).

We now turn to the discussion of the two polymer crystal structures, namely those of P3BT (in form I′) and P3MBT. As mentioned in the Introduction, both polymers crystallize in the orthorhombic $C222_1$ space group. The chains have a planar backbone and they are aligned along the *b* axis. They have an intramolecular 2_1 symmetry element, with the first torsion angle connecting the alkyl side chains to the conjugated backbone at approximately 90°. The polymer chains interact by relatively strong π-staking interactions along the *a* axis, and these stacks are packed to form layers along the *c* axis. The chains within a stack have the same directionality, while the chains belonging to adjacent stacks have opposite directionalities.

In the case of P3MBT (Figure 9 and Table S11 in the Supporting Information), FF1 has both lower rms displacements and lower deviations of the lattice parameters, leading to the smallest *F* value. FF3 is slightly worse, while FF2 has the worst overall performance. In the case of P3BT (Figure 8 and Table S10 in the Supporting Information), FF1 appears to be superior for Δ_{rms}(ao), while FF2 leads to better lattice parameters. However, the *F* value indicates that the best overall results are obtained with FF3. So here we have one important case where FF3 does not fall between FF1 and FF2, but outperforms both of them. This is seen also in the MD simulations, which will be presented below.

In the case of α-quaterthiophene (T4) and α-sexithiophene (T6), the energies obtained from the crystal structure optimizations can used to also compute their heats of sublimation, which have been measured experimentally.[54] We computed the heats of sublimation from

$$\Delta H^0_{subl} \cong U_{gas} - U_{cr} \quad (3)$$

where U_{cr} and U_{gas} are potential energies per mole in the crystal and gas phase (the latter from single-molecule optimization). In eq 3 we have neglected the $p\Delta V$ ($\cong RT$) correction on the right-hand side. This is only 0.6 kcal/mol at 300 K, which is comparable with the experimental uncertainties and accounts for a relatively modest 2−5% of the heats of sublimation. The final results of this calculation are collected in Table 4. We see that FF1 gives heats of sublimation in excellent agreement with experiment, while FF2 tends to overestimate them by about 1 kcal/mol per thiophene ring. Again, FF3 falls somewhere between these two cases.

To summarize, our tests of the force field versions developed in the previous section show that they are all broadly satisfactory for modeling the crystal structures of thiophene-based oligomers and polymers. They reproduce all the crystal structures in our test set, with acceptable deviations from the experimental atomic coordinates and lattice parameters. A detailed comparison has also allowed us to conclude that FF1 is slightly superior for the two polymer structures, but has a somewhat uneven behavior in the oligomer minimizations. FF2 performs better in this respect but, on the other hand, slightly overestimates the heats of sublimation of **T4** and **T6**. Quite predictably, FF3 interpolates between these two extremes.

4. Molecular Dynamics Simulations

Having assessed the overall reliability of our force fields in crystal structure minimizations, we briefly illustrate their application in MD simulations. For this purpose, we have chosen the two polymers[15,17] and tetrahexylsexithiophene, which may crystallize in the "yellow" form (LIWRAK[49]) or in the "red" form (LIWRAK01[50]). Note that the polymer chains have no terminations and therefore they are infinitely long in our models. Also, we point out that our polymer crystal models are infinitely large, because of the three-dimensional periodicity adopted in the simulations. Instead, it is well-known that polymers and in particular poly(alkylthiophenes) are semicrystalline, with a sizable amount of amorphous material. The crystallite sizes inferred from the Rietveld analysis of the X-ray data (coherence lengths, related to the diffraction peak widths) are typically of the order of a few nanometers. Such problems do not usually exist in the case of the oligomers, where relatively large crystals suitable for single-crystal X-ray diffraction can often be prepared. In particular, the structure of LIWRAK was determined in this way. Instead, the solution of the structure of LIWARK01 was more laborious and required a combination of powder X-ray analysis, Monte Carlo simulated annealing and density functional calculations. The final structure was characterized by some thermal disorder, which was modeled by fractional occupations of the atomic positions.[50] All this should be borne in mind when comparing to the experimental data.

For both P3BT and P3MBT, we simulated a 6 × 6 × 2 supercell. For LIWRAK and LIWRAK01, we took a 8 × 3 × 3 and a 2 × 6 × 3 supercell, respectively. These choices produce systems with about 10^4 atoms and box sides of 40−50 Å. The equations of motion were integrated by the Velocity Verlet algorithm with a 2 fs time step, having eliminated the fast

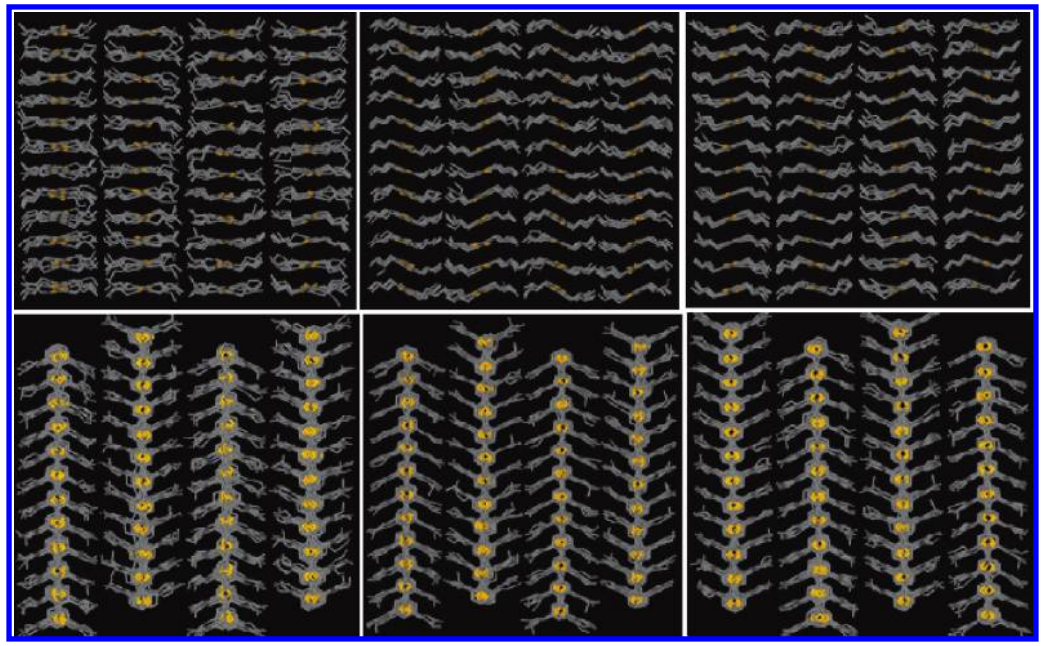

Figure 10. Snapshots from the MD simulations of a 6 × 6 × 2 supercell of P3BT (form I′). From left to right, we show configurations obtained with FF1, FF2, and FF3. The crystals are viewed along the *b* axis in the top row and along the *a* axis in the bottom row. Hydrogens have been omitted for clarity.

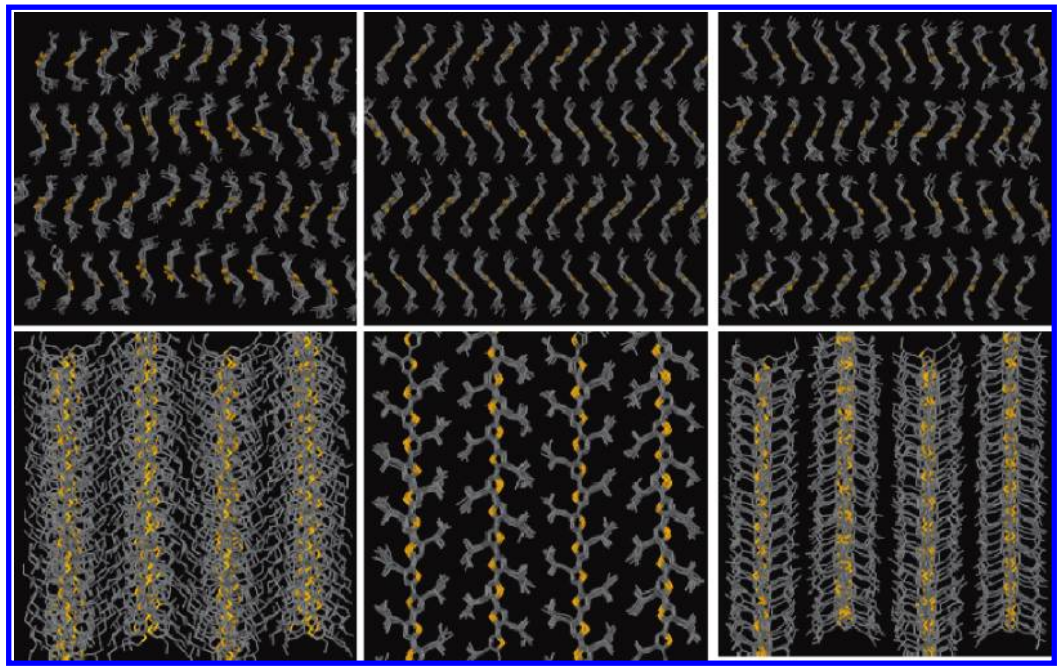

Figure 11. Snapshots from MD simulations of a 6 × 6 × 2 supercell of P3MBT. From left to right, we show configurations obtained with FF1, FF2, and FF3. The crystals are viewed along the *b* axis in the top row and along the *a* axis in the bottom row. Hydrogens have been omitted for clarity.

vibration of all C−H bonds by use of the RATTLE algorithm. The loose coupling method of Berendsen et al.[55] was used to control both temperature and pressure, which were set to 300 K and 1.0 atm, respectively. The default relaxation times $\tau_T = 0.2$ ps and $\tau_P = 2$ ps were used for the thermostat and barostat. Following the original treatment,[55] the DYNAMIC program of TINKER was modified in order to allow changes of all lattice parameters, away from the experimental values. In the polymer simulations, the lattice lengths were allowed to fluctuate independently, while the lattice angles were kept fixed at the orthorhombic values $\alpha = \beta = \gamma = 90°$ (as in the original unit cells). Instead, in the oligomer simulations we adopted a triclinic simulation box, allowing full independent fluctuations of both lattice lengths and lattice angles. Starting from an experimental structure, the equilibrium values of the lattice parameters are reached fairly quickly (typically in less than 50 ps) and they are then retained for the remainder of the simulation (500−2000 ps, overall).

We start by discussing the MD simulations of the two polymers. Figures 10 and 11 provide snapshots of the final system configurations, for each force field. The equilibrium lattice parameters (multiples of the unit cell parameters) and their standard deviations are given in Tables 5 and 6. The last line in the tables contains the *F* values, calculated from the average lattice parameters by an equation analogous to eq 2, excluding the contribution from the atomic mean-square dis-

TABLE 5: Average Lattice Parameters and Standard Deviations (in Å) and *F* Parameter Value, from the MD Simulations of P3BT at 300 K and 1 atm

	exptl	FF1	FF2	FF3
$6 \times a$	45.84	45.33 ± 0.09	48.14 ± 0.06	45.94 ± 0.03
$6 \times b$	46.50	46.74 ± 0.01	46.77 ± 0.006	46.77 ± 0.005
$2 \times c$	49.94	54.49 ± 0.09	52.23 ± 0.06	53.92 ± 0.08
F	—	84.51	46.54	63.90

TABLE 6: Average Lattice Parameters and Standard Deviations (in Å) and *F* Parameter Value, from the MD Simulations of P3MBT at 300 K and 1 atm

	exptl	FF1	FF2	FF3
$6 \times a$	49.45	57.18 ± 0.09	56.42 ± 0.05	53.63 ± 0.08
$6 \times b$	46.50	46.43 ± 0.007	46.68 ± 0.006	46.66 ± 0.006
$2 \times c$	54.00	48.28 ± 0.08	49.21 ± 0.06	51.70 ± 0.06
F	—	356.58	277.50	89.71

placements. As expected, the *b* axis (chain axis) is always reproduced very well by all force fields. Instead, there are more significant changes along the *a* axis (the π-stacking direction) and along the *c* axis (the layering direction).

In P3BT (Figure 10 and Table 5), we see that FF1 and FF3 predicts a 8−9% expansion of *c*, while FF2 predicts a 4−5% expansion of both *a* and *c*. After accounting for thermal expansion, these behaviors are in line with the differences which emerged from the energy minimizations. If we look at the final snapshots of the systems, we see that the original crystal structure is roughly conserved after the introduction of thermal motions, but with some clearly visible differences. With FF1, the alkyl side chains are somewhat more disordered and the π-conjugated backbones have lost their characteristic tilting with respect to the stacking direction. Both the main and the side chains appear more ordered with FF2 and FF3. Even in this case, however, there is a clearly visible population of gauche conformations at the ends of the alkyl chains, where two π-staked layers meet.

In P3MBT (Figure 11 and Table 6), FF1 and FF2 predict comparable variations of the lattice parameters: *a* expands by about 12%, *c* contracts by 10%, leading to large *F* values. However, these variations are accompanied by very different chain arrangements. With FF1 we have a fairly disordered system, where both the main chains and the side chains show significant departures from their original equilibrium positions. On the contrary, the FF2 simulations predict a very ordered system. Here, however, the main chains have shifted along their axes, bringing the π-stacked thiophene rings and their side chains into an "eclipsed" configuration. This is not consistent with the experimental structure. Thus, in this case we have a strong indication that FF1 and FF2 underestimate and overestimate chain−chain interactions, respectively. FF3, which was defined as their "average", leads to a much better set of lattice parameters and a much lower *F* value, presumably because it captures the right amount of structural freedom in the crystal.

Figures 12 and 13 illustrate our results for the MD simulations of LIWRAK and LIWRAK01. Tables 7 and 8 collect the quantitative data on the equilibrium lattice parameters. We see that they all provide an excellent description of the first structure. Note that its final *F* values (17−20) are much lower than those extracted from the MM minimizations described in the previous

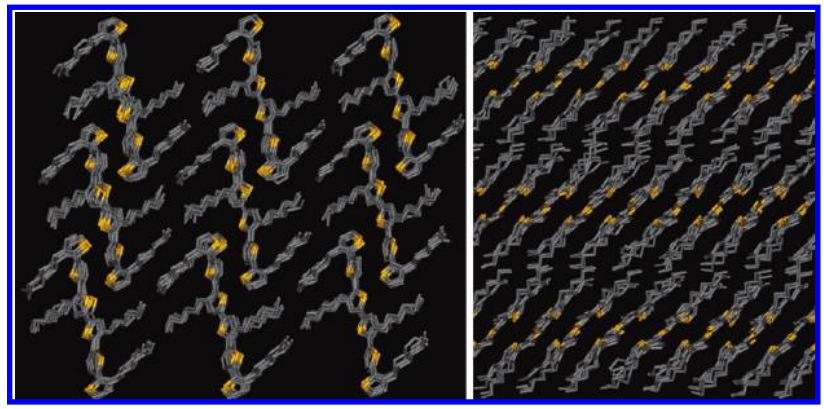

Figure 12. Views along the *a* axis (left) and the *b* axis (right) of a representative configuration of LIWRAK at 300 K and 1 atm, obtained from the MD simulations with FF3. Hydrogens have been omitted for clarity.

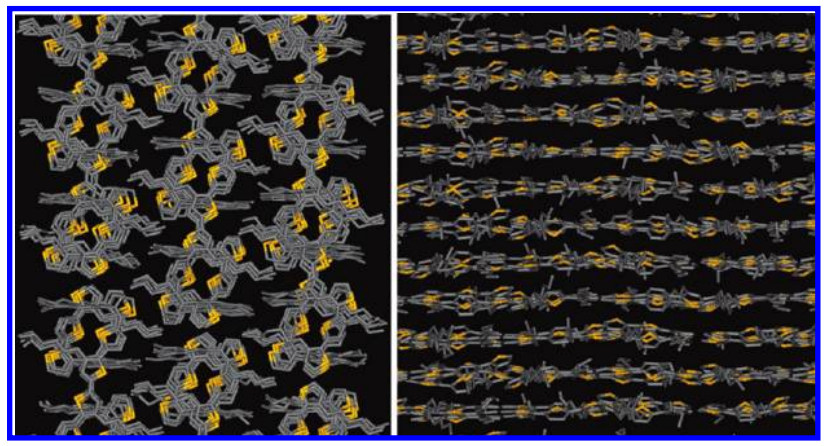

Figure 13. Views along the *b* axis (left) and the *c* axis (right) of a representative configuration of LIWRAK01 at 300 K and 1 atm, obtained from the MD simulations with FF3. Hydrogens have been omitted for clarity.

TABLE 7: Average Lattice Parameters and Standard Deviations (in Å) and *F* Parameter Value, from the MD Simulations of LIWRAK at 300 K and 1 atm

	exptl	FF1	FF2	FF3
$8 \times a$	43.94	44.85 ± 0.09	44.61 ± 0.05	44.57 ± 0.09
$8 \times b$	40.73	39.87 ± 0.04	40.05 ± 0.02	39.99 ± 0.04
$3 \times c$	49.36	49.39 ± 0.04	48.76 ± 0.04	49.07 ± 0.08
α	102.46	99.86 ± 0.07	99.84 ± 0.07	99.80 ± 0.12
β	92.54	92.78 ± 0.07	93.14 ± 0.07	92.93 ± 0.08
γ	100.86	99.55 ± 0.19	98.23 ± 0.09	98.54 ± 0.15
F	—	16.94	20.35	17.91

TABLE 8: Average Lattice Parameters and Standard Deviations (in Å) and *F* Parameter Value, from the MD Simulations of LIWRAK01 at 300 K and 1 atm

	exptl	FF1	FF2	FF3
$2 \times a$	49.90	46.90 ± 0.06	46.86 ± 0.07	46.82 ± 0.05
$6 \times b$	45.09	50.09 ± 0.08	49.25 ± 0.06	49.61 ± 0.12
$3 \times c$	41.61	40.71 ± 0.09	40.95 ± 0.05	40.94 ± 0.06
α	90.00	90.41 ± 0.21	89.77 ± 0.29	90.88 ± 0.15
β	117.24	114.06 ± 0.17	114.01 ± 0.12	114.05 ± 0.15
γ	90.00	89.39 ± 0.31	90.81 ± 0.27	89.94 ± 0.46
F	—	171.81	133.21	149.54

section (87−95). Thus, the MD simulations of this system capture very well its (anisotropic) thermal expansion. The simulations reproduce also the distortion from planarity of the terminal backbone dihedrals, which characterizes this structure. The description of the second polymorph is not equally satisfactory, but it is nonetheless acceptable. Inspection of Figure 9 (obtained with FF3, but representative also of the behavior of FF1 and FF2) provides a visual demonstration of the larger degree of thermal disorder in this system, in agreement with the proposed experimental structure.[50]

5. Conclusions

We have developed and thoroughly tested a series of closely related force fields for the simulation of alkylthiophene-based oligomers and polymers. These force fields depend on different choices for the atomic charges entering the calculation of the electrostatic interactions. Force field FF1 is based on a simple extension of the charge set adopted by OPLS-AA, while FF2 builds on ab initio electrostatic potential fits for a few representative oligomers. Each has its strengths and weaknesses. The best overall results are obtained with force field FF3, where we simply averaged the atomic charges from the former two. While this does not outperform the others on each of the investigated systems (in fact, either FF1 or FF2 is usually better when tested on a single structure), it provides a more balanced overall description. This is confirmed by adding up all the tabulated *F* values from the MM and MD simulations in the previous sections: we obtain 1551 for FF1, 1048 for FF2 and the lowest (i.e., best) value of 996 for FF3.

A second important result from this molecular modeling study is that the crystal structures of P3MBT and P3BT previously reported by our group have been confirmed to be stable also at room temperature, and therefore they correspond to well-defined energetic minima. Our MD simulations show that these systems contain a certain degree of conformational disorder in the side chains, even under the present implied assumption that these polymeric crystals are virtually defect-free and infinite in size. We have also shown that a comparable or even greater amount of disorder may be present in some of the oligomeric systems, depending on their specific molecular packing conditions. This feature, together with the presence of a not-so-stiff π-conjugated backbone and several types of competing intermolecular interactions, has made the accurate modeling of these polyconjugated systems with alkyl side chains a challenging task.

While the present results represent a step forward in the quantitative description of these systems by MM force fields, we do not expect them put the word "end" to it. The analogous parametrization of biomolecular force fields has required several years of work by a much larger community, and it is still an ongoing effort. In this context, there have been several recent attempts to go beyond the static point charge model,[31] for example, through the incorporation of atomic multipole moments and polarizabilities.[23] At some stage, this will probably have to be done also for these π-conjugated systems. Approximate electronic structure methods suitable for very large systems would be even better. At the other extreme, there is clearly a need of a chemically realistic coarse-grained model for the simulation of their large-scale and long-time properties.[56] In the meantime, we hope that our work will be a useful tool in the hands of all those interested in the simulation of thiophene-based materials. We envisage their application as an aid to polymer crystal structure determination, in the simulation of polythiophene self-assembly in solution and on solid surfaces, in the description of molecular arrangements in blends such as those of bulk heterojunction solar cells, and to generate realistic polymer configurations for the calculation of charge and excitation transport.

Acknowledgment. This work was financially supported by ENI and by INSTM (PRISMA grant to G.R.).

Supporting Information Available: Force field parameter file for FF3, in TINKER format. Pictures of all the crystal structures and tables summarizing the optimization results. This material is available free of charge via the Internet at http://pubs.acs.org.

References and Notes

(1) Roncali, J. *Chem. Rev.* **1997**, *97*, 173.
(2) *Electronic Materials: The Oligomer Approach*; Müllen, K., Wegner G., Eds.; Wiley-VCH: Weinheim, Germany, 1998.
(3) *Handbook of Oligo-and Polythiophenes* (Fichou, D. Ed.), Wiley-VCH, Weinheim, 1999.
(4) Fichou, D. *J. Mater. Chem.* **2000**, *10*, 571.
(5) Mena-Osteritz, E. *Adv. Mater.* **2002**, *14*, 609.
(6) Osaka, I.; McCullough, R. D. *Acc. Chem. Res.* **2008**, *41*, 1202.
(7) *Handbook of Thiophene-Based Materials*; Perepichka, I. F., Perepichka D. F., Eds.; Wiley-Blackwell: Chirchester, UK, 2009; Vol. 1 and 2.
(8) (a) Katz, H. E.; Bao, Z. *J. Phys. Chem. B* **2000**, *104*, 671. (d) Dimitrakopoulos, C. D.; Malefant, P. R. L. *Adv. Mater.* **2002**, *14*, 99.
(9) (a) Kraft, A.; Grimsdale, A. C.; Holmes, A. B. *Angew. Chem., Int. Ed.* **1998**, *37*, 402. (b) Köhler, A.; Wilson, J. S.; Friend, R. H. *Adv. Mater.* **2002**, *14*, 701.
(10) (a) McQuade, D. T.; Pullen, A. E.; Swager, T. M. *Chem. Rev.* **2000**, *100*, 2537. (b) Barbarella, G.; Melucci, M.; Sotgiu, G. *Adv. Mater.* **2005**, *17*, 1581.
(11) (a) Günes, S.; Neugebauer, H.; Sariciftci, N. S. *Chem. Rev.* **2007**, *107*, 1324. (b) Thompson, B. C.; Fréchet, J.-M. *Angew. Chem., Int. Ed.* **2008**, *47*, 58. (c) Po, R.; Maggini, M.; Camaioni, N. *J. Phys. Chem. C*, DOI 10.1021/jp9061362.
(12) (a) Barbara, P. F.; Meyer, T. J.; Ratner, M. A. *J. Phys. Chem.* **1996**, *100*, 13148. (b) Brédas, J.-L.; Beljonne, D.; Coropceanu, V.; Cornil, J. *Chem. Rev.* **2004**, *104*, 4971. (c) Coropceanu, V.; Cornil, J.; da Silva Filho, D. A.; Olivier, Y.; Silbey, R.; Brédas, J.-L. *Chem. Rev.* **2007**, *107*, 926. (d) Nelson, J.; Kwiatkowski, J. J.; Kirkpatrick, J.; Frost, J. M. *Acc. Chem. Res.* **2009**, *42*, 1768.
(13) Nitzan, A. *Chemical Dynamics in Condensed Phases*; Oxford University Press: Oxford, UK, 2006.
(14) (a) Winokur, M. J.; Wamsely, P.; Moulton, J.; Smith, P.; Heeger, A. J. *Macromolecules* **1991**, *24*, 3812. (b) Prosa, T. J.; Winokur, M. J.; Moulton, J.; Smith, P.; Heeger, A. J. *Macromolecules* **1992**, *25*, 4364. (c) Prosa, T. J.; Winokur, M. J.; Moulton, J.; Smith, P. *Synth. Met.* **1993**, *55*, 370. (d) Prosa, T. J.; Winokur, M. J.; McCullogh, R. D. *Macromolecules*

1996, *29*, 3654. (e) Tashiro, K.; Ono, K.; Minagawa, Y.; Kobayashi, M.; Kawai, T.; Yoshino, K. *J. Polym. Sci., Part B: Polym. Phys.* **1991**, *29*, 1223. (f) Tashiro, K.; Kobayashi, M.; Morito, S.; Kawai, T.; Yoshino, K. *Synth. Met.* **1995**, *69*, 397. (g) Mardalen, J.; Samuelsen, E. J.; Gautun, O. R.; Carsen, P. H. *Solid State Commun.* **1991**, *77*, 337. (h) Mardalen, J.; Samuelsen, E. J.; Gautun, O. R.; Carlsen, P. H. *Synth. Met.* **1992**, *48*, 363. (i) Bolognesi, A.; Catellani, M.; Destri, S.; Porzio, W. *Makromol. Chem. Rapid Commun.* **1991**, *12*, 9. (j) Bolognesi, A.; Porzio, W.; Provasoli, F.; Ezquerra, T. *Makromol.Chem.* **1993**, *194*, 817. (k) Meille, S. V.; Romita, V.; Caronna, T.; Lovinger, A. J.; Catellani, M.; Belobrzeckaja, L. *Macromolecules* **1997**, *30*, 7898. (l) Malik, S.; Nandi, A. K. *J. Pol. Science: Part B: Pol. Phys.* **2002**, *40*, 2073. (m) Causin, V.; Marega, C.; Marigo, A.; Valentini, L.; Kenny, J. M. *Macromolecules* **2005**, *38*, 409. (n) Zen, A.; Saphiannikova, M.; Neher, D.; Grenzer, J.; Grigorian, S.; Pietsch, U.; Asawapirom, U.; Janietz, S.; Scherf, U.; Lieberwirth, I.; Wegner, G. *Macromolecules* **2006**, *39*, 2162. (o) Zhang, R.; Li, B.; Iovu, M. C.; Jeffries-EL, M.; Sauvé, G.; Cooper, J.; Jia, S.; Tristam-Nagle, S.; Smilgies, D. M.; Lambeth, D. N.; McCullough, R. D.; Kowalewski, T. *J. Am. Chem. Soc.* **2006**, *128*, 3480. (p) Brinkmann, M.; Rannou, P. *Adv. Funct. Mater.* **2007**, *17*, 101. (q) Kline, J.; McGehee, M. D.; Kadnikova, E. N.; Liu, J.; Fréchet, J. M. *Adv. Mater.* **2003**, *15*, 1519. (r) Lu, G. H.; Li, L. G.; Yang, X. N. *Adv. Mater.* **2007**, *19*, 3594. (s) Lu, G. H.; Li, L. G.; Yang, X. N. *Macromolecules* **2008**, *41*, 2062.

(15) Arosio, P.; Famulari, A.; Catellani, M.; Luzzati, S.; Torsi, L.; Meille, S. V. *Macromolecules* **2007**, *40*, 3.

(16) (a) Rietveld, H. M. *Acta Crystallogr.* **1966**, *20*, 508. (b) Rietveld, H. M. *Acta Crystallogr.* **1967**, *22*, 151.

(17) Arosio, P.; Famulari, A.; Moreno, M.; Raos, G.; Catellani, M.; Meille, S. V. *Chem. Mater.* **2009**, *21*, 78.

(18) Corradini, P. Chain Conformation and Crystallinity. In *The Stereochemistry of Macromolecules*; Ketley, A. D., Ed.; M. Dekker: New York, 1968; Vol. 3, p 1.

(19) Allen, M. P.; Tildesley, D. J. *Computer Simulation of Liquids*; Oxford University Press: New York, 1987.

(20) Leach, A. R. *Molecular Modelling: Principles and Application*, 2nd ed.; Prentice Hall: London, 2001.

(21) Field, M. J. *A Practical Introduction to the Simulations of Molecular Systems*, 2nd ed.; Cambridge University Press: Cambridge, UK, 2007.

(22) Koch, W.; Holthausen, M. C. *A Chemist's Guide to Density Functional Theory*; Wiley-VCH: Weinheim, Germany, 2001.

(23) Stone, A. J. *The Theory of Intermolecular Forces*; Clarendon Press: Oxford, UK, 1996.

(24) Marcon, V.; Raos, G. *J. Phys. Chem. B* **2004**, *108*, 18053.

(25) (a) Marcon, V.; Raos, G.; Allegra, G. *Macromol. Theory Simul.* **2004**, *13*, 497. (b) Campione, M.; Sassella, A.; Moret, M.; Papagni, A.; Trabattoni, S.; Resel, R.; Lengyel, O.; Marcon, V.; Raos, G. *J. Am. Chem. Soc.* **2006**, *128*, 13378. (c) Marcon, V.; Raos, G.; Campione, M.; Sassella, A. *Cryst. Growth Des.* **2006**, *6*, 1826. (d) Marcon, V.; Raos, G. *J. Am. Chem. Soc.* **2006**, *128*, 1408.

(26) (a) Gus'kova, O. A.; Mena-Osteritz, E.; Schillinger, E.; Khalatur, P. G.; Bäuerle, P.; Khokhlov, A. R. *J. Phys. Chem. C* **2007**, *111*, 7165. (b) Gus'kova, O. A.; Khalatur, P. G.; Khokhlov, A. R. *Macromol. Theory Simul.* **2009**, *18*, 219.

(27) (a) Cheung, D. L.; McMahon, D. P.; Troisi, A. *J. Phys. Chem. B* **2009**, *113*, 9393. (b) Cheung, D. L.; McMahon, D. P.; Troisi, A. *J. Am. Chem. Soc.* **2009**, *131*, 11179.

(28) Vukmirovic, N.; Wang, L.-W. *J. Phys. Chem. B* **2009**, *113*, 409.

(29) Curcó, D.; Alemán, C. *J. Comput. Chem.* **2007**, *28*, 1743.

(30) Widge, A. S.; Matsuoka, Y.; Kurnikova, M. *J. Mol. Graph. Mod.* **2008**, *27*, 34.

(31) Ponder, J. W.; Case, D. A. *Adv. Protein Chem.* **2003**, *66*, 27.

(32) (a) Jorgensen, W. L.; Maxwell, D. S.; Tirado-Rives, J. *J. Am. Chem. Soc.* **1996**, *118*, 11225. (b) Jorgensen, W. L.; Tirado-Rives, J. *Proc. Natl. Acad. Sci.* **2005**, *102*, 6665.

(33) MacKerell, A. D., Jr. *J. Phys. Chem. B* **1998**, *102*, 3586.

(34) Cornell, W. D.; Cieplak, P.; Bayly, C. I.; Gould, I. R.; Merz, K. M.; Ferguson, D. M.; Spellmeyer, D. C.; Fox, T.; Caldwell, J. W.; Kollman, P. A. *J. Am. Chem. Soc.* **1995**, *117*, 5179.

(35) (a) Allinger, N. L.; Yuh, Y. H.; Li, J.-H. *J. Am. Chem. Soc.* **1989**, *111*, 8551. (b) Li, J.-H.; Allinger, N. L. *J. Am. Chem. Soc.* **1989**, *111*, 8566 and 8576. (c) Yang, L.; Allinger, N. L. *THEOCHEM* **1996**, *370*, 71.

(36) (a) Agosti, E.; Rivola, M.; Hernandez, V.; Del Zoppo, M.; Zerbi, G. *Synth. Met.* **1999**, *100*, 101. (b) Degli Esposti, A.; Zerbetto, F. *J. Phys. Chem. A* **1997**, *101*, 7283.

(37) Ponder, J. W. *TINKER: Software Tools for Molecular Design*, 4.2th ed.; Washington University School of Medicine: Saint Louis, MO, 2003. Available from http://dasher.wustl.edu/tinker/.

(38) Schmidt, M. W.; Baldridge, K. K.; Boatz, J. A.; Elbert, S. T.; Gordon, M. S.; Jensen, J. H.; Koseki, S.; Matsunaga, N.; Nguyen, K. A.; Su, S. J.; Windus, T. L.; Dupuis, M.; Montgomery, J. A. *J. Comput. Chem.* **1993**, *14*, 411.

(39) Moreno, M.; Castiglione, F.; Mele, A.; Pasqui, C.; Raos, G. *J. Phys. Chem. B* **2008**, *112*, 7826.

(40) Bak, B.; Christensen, D.; Hansen-Nygaard, L.; Rastrup-Andersen, J. *J. Mol. Spectrosc.* **1961**, *7*, 58.

(41) Tsuzuki, S.; Honda, K.; Azumi, R. *J. Am. Chem. Soc.* **2002**, *124*, 12200.

(42) (a) Spackman, M. A. *J. Comput. Chem.* **1996**, *17*, 1. (b) Breneman, C. M.; Wiberg, K. B. *J. Comput. Chem.* **1990**, *11*, 361.

(43) Raos, G.; Famulari, A.; Marcon, V. *Chem. Phys. Lett.* **2003**, *379*, 364.

(44) Van Eijck, L.; Johnson, M. R.; Kearley, G. J. *J. Phys. Chem. A* **2003**, *107*, 8980.

(45) Siegrist, T.; Kloc, C.; Laudise, R. A.; Katz, H. A.; Haddon, R. C. *Adv. Mater.* **1998**, *10*, 379.

(46) Allen, F. H. *Acta Crystallogr., Sect. B: Struct. Sci.* **2002**, *58*, 380.

(47) Horowitz, G.; Bachet, B.; Yassar, A.; Lang, P.; Demanze, F.; Fave, J. L.; Garnier, F. *Chem. Mater.* **1995**, *7*, 1337.

(48) Siegrist, T.; Fleming, R. M.; Haddon, R. C.; Laudise, R. A.; Lovinger, A. J.; Katz, H. E.; Bridenbaugh, P.; Davis, D. *J. Mater. Res.* **1995**, *10*, 2170.

(49) Destri, S.; Ferro, D. R.; Khotina, I. A.; Porzio, W.; Farina, A. *Macromol. Chem. Phys.* **1998**, *199*, 1973.

(50) Neumann, M. A.; Tedesco, C.; Destri, S.; Ferro, D. R.; Porzio, W. *J. Appl. Crystallogr.* **2002**, *35*, 296. In this paper the authors actually discuss three structures, which differ in the choice of the space group. The "best" solution belongs to the *C*2/*m* space group, where the *m* symmetry element was introduced to model thermal disorder effects. As a consequence, all the atomic positions have occupations of 50%. Such fractional occupations cannot be included in MM energy minimizations. Therefore, our MM calculations were started from the "second best" solution, which has a lower symmetry (*C*2 space group) and occupations of 100%.

(51) Kiriy, N.; Kiriy, A.; Bocharova, V.; Stamm, M.; Richter, S.; Plotner, M.; Fischer, W.-J.; Krebs, F. C.; Senkovska, I.; Adler, H.-J. *Chem. Mater.* **2004**, *16*, 4757.

(52) Moret, M.; Campione, M.; Borghesi, A.; Miozzo, L.; Sassella, A.; Trabattoni, S.; Lotz, B.; Thierry, A. *J. Mater. Chem.* **2005**, *15*, 2444.

(53) Azumi, R.; Götz, G.; Debaerdemaeker, T.; Bäuerle, P. *Chem.—Eur. J.* **2000**, *6*, 735.

(54) Kloc, C.; Laudise, R. A. *J. Cryst. Growth* **1998**, *193*, 563.

(55) Berendsen, H. J. C.; Postma, J. P. M.; van Gunsteren, W. F.; DiNola, A.; Haak, J. R. *J. Chem. Phys.* **1984**, *81*, 3684–3690.

(56) Müller-Plathe, F. *ChemPhysChem* **2002**, *3*, 754.

JP9106124